*Aerosol Science and Technology*, 42:395–407, 2008

ISSN: 0278-6826 print / 1521-7388 online
DOI: 10.1080/02786820802104981

# Development and Characterization of a Fast-Stepping/Scanning Thermodenuder for Chemically-Resolved Aerosol Volatility Measurements

**J. Alex Huffman,[1] Paul J. Ziemann,[2] John T. Jayne,[3] Douglas R. Worsnop,[3] and Jose L. Jimenez[1]**

[1]*Department of Chemistry and Biochemistry, and Cooperative Institute for Research in Environmental Sciences (CIRES), University of Colorado, Boulder, Colorado, USA*
[2]*Air Pollution Research Center, University of California, Riverside, California, USA*
[3]*Aerodyne Research Inc., Billerica, Massachusetts, USA*

**A thermodenuder (TD) system, based on the design of Wehner et al. (2002), was designed, constructed, and characterized in the laboratory. The TD consists of a heated tube (2.5 cm ID, 55 cm long) held at a constant temperature by a 3-zone controller, followed by a cooling zone with a diffusion tube lined with activated charcoal for adsorption of evaporated gases. An important improvement over previous designs is the ability to step through TD temperatures in ∼10 min. per step by the reduction of thermal inertia, and the addition of two cooling fans. The TD was characterized in the laboratory, showing that temperature profiles inside are relatively uniform and for response to standard generated particle species. Losses at ambient temperature are close to diffusion losses estimated with literature techniques and to those experimentally measured by Wehner et al. Particle number losses are observed to increase for volatile species upon heating due to particles shrinking to sizes where diffusion and thermophoresis are more efficient. The thermodenuder was placed upstream of an Aerodyne Aerosol Mass Spectrometer (AMS) during several field experiments. An automated valve system was designed and built to allow rapidly alternating data points between thermodenuder-processed aerosol and un-processed aerosol. This system has enabled the rapid (1–3 h) collection of chemically-resolved volatility over the range of 54–230°C in the field for the first time. Examples of field data are shown where the species volatilities vary as expected.**

Received 5 December 2007; accepted 4 April 2008.

The authors would like to thank Allison Aiken, Kenneth Docherty, Ingrid Ulbrich, Peter DeCarlo, Joel Kimmel, Ed Dunlea, Michael Cubison, Achim Trimborn, Jesse Kroll, Megan Northway, and Dara Salcedo for assistance in collecting data, and Timothy B. Onasch for useful discussions. We also thank the organizers of MILAGRO (S. Madronich and L. Molina) and FLAME (S. Kreidenweis, C. Wold, W. Hao, and W. Malm). These studies were partially supported by grants DOE (BER, ASP Program) DEFG02-05ER63981, EPA STAR R831080 and RD-83216101-0, NSF ATM-0449815 and ATM-0528634, NASA NNG04GA67G, EPA R833747 and by a NASA fellowship NGT5-30516 to JAH. This article has not been reviewed by either funding agency and thus no official endorsement should be inferred.

Address correspondence to Jose L. Jimenez, Department of Chemistry and Biochemistry, and Cooperative Institute for Research in Environmental Sciences (CIRES), University of Colorado, Boulder, Colorado, 80309. E-mail: jose.jimenez@colorado.edu

## INTRODUCTION

Atmospheric aerosols can have important effects on global climate radiative forcing (IPCC 2007), negative effects on human health (Davidson et al. 2005), visibility reduction (Watson 2002), and deposition to terrestrial systems (Likens et al. 1996). Their short lifetimes and wide range of particle sizes, chemical compositions, and physical properties, however, make comprehensive study of atmospheric aerosols very complex (McMurry 2000). Volatility is an important physical property, which is defined by the chemical properties of the condensed species and may reflect some chemical history of the particle (Jonsson et al. 2007). Photochemical reactions in the atmosphere can change the chemical functionality of gaseous species, lowering their vapor pressures to the point where they partition into the particle phase (Went 1960), and thus contributing significantly to global aerosol concentrations (e.g., Kanakidou et al. 2005). Particle volatility directly influences the lifetimes of chemical species in the atmosphere not only by removal through secondary reactions, but through widely different removal rates for wet and dry deposition processes for gases vs. particles (Franz et al. 1998; Simcik et al. 1998). Aerosol volatility can also help define the levels of vapor reemission from particles deposited to terrestrial surfaces (Daly and Wania 2004). Some species may condense upon cooling when lofted into the free troposphere (Kanakidou et al. 2005), or evaporate when concentrated pollution plumes are heated or diluted with less polluted airmasses (Lipsky and Robinson 2006; Shrivastava et al. 2006). Finally, knowledge of volatility can aid the estimation of particle losses in aircraft sampling inlets (Wilson and Seebaugh 2001) and within particle sampling instruments (e.g., Meyer et al. 2000).

The measurement and analysis of aerosol volatility, which has also been called thermal fractionation (Hudson and Da 1996), takes advantage of the fact that different chemical species will evaporate rapidly at characteristic temperatures related to their vapor pressures, boiling points, and enthalpies of vaporization (e.g. Burtscher et al. 2001; Kreidenweis et al. 1998; Villani et al. 2007). As the particles are heated, the more volatile species evaporate preferentially leaving behind the less volatile species still in the particle phase. This technique has been utilized for decades to gain indirect information about aerosol physical and especially chemical characteristics when not easily measurable otherwise. Goetz et al. (1961) measured the decreasing particle size as foil samples of collected ambient particles were heated. The use of a heated volatilization flowtube to evaporate particle material for direct in situ analysis dates back at least to Twomey (1968; 1971b), who inferred the composition of cloud condensation nuclei (CCN) in the NE United States to be mostly sulfate from measured particle volatility. In order to infer particle composition, later studies also placed a heated tube upstream of a: thermal-expansion cloud chamber (Dinger et al. 1970; Hoppel et al. 1973; Twomey 1971a), photoelectric particle counter (Rosen 1971), nephelometer (Husar and Shu 1975; Pueschel et al. 1973), and light-scattering aerosol spectrometer (Jennings and O'Dowd 1990; Pinnick et al. 1987). Study of inferred aerosol composition has also focused on the separation of elemental species that remain in the particle phase at high temperature (800°C and above) from more volatile species (Jennings et al. 1994; Smith and O'Dowd 1996). Techniques to speciate aerosol sulfate more directly were developed by adding selective gas denuders to heated flowtubes for detection by: flame photometry (Cobourn et al. 1981; Tanner et al. 1980), and nephelometry (Larson et al. 1982; Ten Brink et al. 1996).

The general idea of placing a heated flowtube upstream of detecting instrumentation has gone by several names and here is referred to as a thermodenuder (TD). Most TDs have been quartz (e.g., Twomey 1971b) or stainless steel (e.g. Burtscher et al. 2001) tubes wrapped in some form of heating tape or placed in an oven (An et al. 2007), leading downstream to the detecting instruments. Clarke (1991) further developed the technique to allow for rapid volatility analysis in aircraft by placing six heated tubes in parallel and measuring the resultant size-distributions with a custom laser aerosol spectrometer. By placing a heated tube, or several in parallel, between two differential mobility analyzers (DMAs) one can measure the size reduction of size-resolved particles upon heating. These instruments are referred to as volatility tandem DMAs (VTDMAs) and have been widely used in several forms (Brooks et al. 2002; Kuhn et al. 2005; Orsini et al. 1999; Philippin et al. 2004; Villani et al. 2007). Recently VTDMAs have been employed to help investigate the volatility and composition of chamber-generated organic aerosol particles in several studies (Baltensperger et al. 2005; Jonsson et al. 2007; Kalberer et al. 2004; Offenberg et al. 2006; Paulsen et al. 2006; Stanier et al. 2007).

Burtscher et al. (2001) built upon the thermodenuder concept (Jennings and O'Dowd, 1990; Pinnick et al. 1987; Twomey 1971b) using a metal tube wrapped in heating tape, but optimized the instrument for experiments where organic particle concentrations are high. To reduce the chemical interference from gas recondensation, Burtscher et al. added a charcoal denuder immediately downstream of the volatilization tube. This section allows gas vapors volatilized in the heating section a surface on which to adsorb upon cooling, further ensuring that the remaining signal is dominated by the less volatile particle species. These authors characterized their instrument both theoretically and experimentally for temperature stability, particle losses, gas recondensation, and with respect to known compounds. Wehner et al. (2002) further improved upon the Burtscher et al. and earlier designs by improving the uniformity of the temperature profile and adding sufficient residence time for adequate evaporation of particle species. This design has been utilized for measurements of ambient (Ehn et al. 2007; Wehner et al. 2005; 2004) and vehicle combustion exhaust (Schneider et al. 2005) aerosol volatility, but only at a single set temperature of 280–300°C. An et al. (2007) utilized the general designs of Burtscher et al. and Wehner et al. and further developed a new TD design that exhibits high temperature stability, but low temperature-ramping speed due to its placement in a tube furnace. They investigated the role of residence time on particle evaporation and concluded that many TD designs can under-predict particle volatility by not allowing adequate time for mass transfer kinetics to act and approach equilibrium.

The TD discussed here was developed to add volatility as an additional dimension of separation for datasets from the Aerodyne Aerosol Mass Spectrometer (AMS) (Canagaratna et al. 2007; Jayne et al. 2000; Jimenez et al. 2003) and similar instruments. The AMS has high time resolution (DeCarlo et al. 2006) and performs ensemble averages of particle concentration and composition, typically between 1 and 5 minute averages during normal operation. It can provide the concentrations of non-refractory inorganic species as well as of several types of organic species based on factor analysis of organic spectra (Zhang et al. 2007, 2005). The High-Resolution Time-of-Flight AMS (HR-ToF-AMS) is a recently developed version of the AMS, which provides additional chemical resolution due to the use of a high resolution mass spectrometer (DeCarlo et al. 2006). Adding the TD in series in front of a chemical analyzer allows the detailed analysis of chemically-resolved volatility, which represents a significant advance from the use of volatility data to infer limited chemical composition information. To our knowledge this is the first such application for ambient analysis. This technique may allow further classification of organic aerosols if components which are difficult to separate due to their similar mass spectra have some differences in volatility that can be exploited by component analysis techniques.

## METHODS AND INSTRUMENT DESIGN

A thermodenuder was designed and constructed based on the published design of Wehner et al. (2002), who improved on earlier designs by providing a more uniform temperature profile and increased residence time for evaporation of particle species. Figure 1 shows a schematic of the improved design discussed here. The heating stage consists of a 1 inch OD (2.5 cm), 0.875 inch ID (2.2 cm) stainless steel tube 55 cm in length, which is wrapped with three fiberglass-coated heating tapes (Thermolyne, 60 cm long). The tube and heating tapes are then wrapped with ∼0.5 inch (1.3 cm) fiberglass insulation and covered with 6 inch OD (15 cm) stainless steel stove pipe as an outer casing. The heating tube passes through a 0.5 inch (1.3 cm) aluminum plate at either end, which hold the tube in place. Two fans (4.7 $ft^3$/min) are installed in the outer casing of the heating section and can be used to blow air through the volume surrounding the heated aerosol tube to cool the unit at a faster rate. During this operation one fan pulls air into the volume, and the second forces heated air out. Each of the three heating zones is temperature controlled by a PID hardware controller (Newport temperature controller, i8; PID Settings of: 10, 100, and 300) whose set-point is computer-controlled with a USB connection and can be set independently from one another to achieve a flatter overall profile. The temperature controllers and the fans can be operated manually, or by software during automated operation. The first (heating) stage is joined to the second (denuding) stage by a 1 to 3/4 inch (2.5 to 1.9 cm) Swagelok reducing union. The denuding stage is constructed exactly like a diffusion drier, with activated carbon charcoal replacing the silica gel and solid aluminum walls replacing the clear plastic walls. It consists of a 0.75 inch ID (1.9 cm) mesh tube held in place at either end by 0.75 inch OD (1.9 cm) tubes affixed to the end caps. These caps are attached to the body-wall of the denuder with Viton o-rings to provide an air-tight seal. The volume outside of the mesh is filled with activated carbon charcoal (Fisherbrand, 6–14 Mesh).

The main difference in our design objectives versus those of previous designs is that our TD was designed with additional temperature control and reduced thermal mass in order to allow for temperature-stepping. This design change included the use of three controllers, the replacement of the sand insulation of Wehner et al. with the looser and less massive fiberglass insulation, and the addition of cooling fans allows for faster temperature changes. Rapid stepping allows one to obtain information about a wide range of volatilities on a time scale comparable to or shorter than most aerosol variations in ambient air.

The rapid measurement of volatility also requires the interleaved measurement of non-evaporated ambient particles. A valve system was designed to allow for automatic switching between sampling states. During typical operation, aerosol is pulled from an inlet and split into two streams, each passing through a Swagelok ball valve controlled by a computer-controlled DC-actuator (Swagelok, MS-141DC). The valve states determine whether the TD-processed aerosol or the unprocessed aerosol is sent to the detection instrumentation. The other stream is pulled through a critical orifice into a sampling pump (Gast oil-free vacuum pump) in order to maintain a constant flow through the denuder and the rest of the sampling system. Figure 1 shows the valve configuration during each sampling state.

The flowrate, as determined by the work of Wehner et al. (2002), is set to a constant 0.6 lpm (at ambient temperature). The flow is laminar (Re = 38), and the air residence time (RT) at ambient temperature calculated as a plug flow (plug flow RT or PFRT) is 21.2 seconds through the 55 cm heating zone, or 10.6 seconds calculated as a minimum time at the centerline of the laminar flow velocity profile (centerline RT or CLRT). Because the airflow needs some linear distance within the heating zone to reach the setpoint (see following section), the effective PFRT at that temperature is ∼15 s. The air density in the volatilization tube is temperature-dependent, however, and will therefore force a temperature-dependent velocity increase (Villani et al. 2007). At 54°C (±6.5%) the PFRT over the length of the heating zone is 11.9 s, but only 7.9 s at 230°C (±15°C or 6.5%). Kinetic limitations of residence time and evaporation

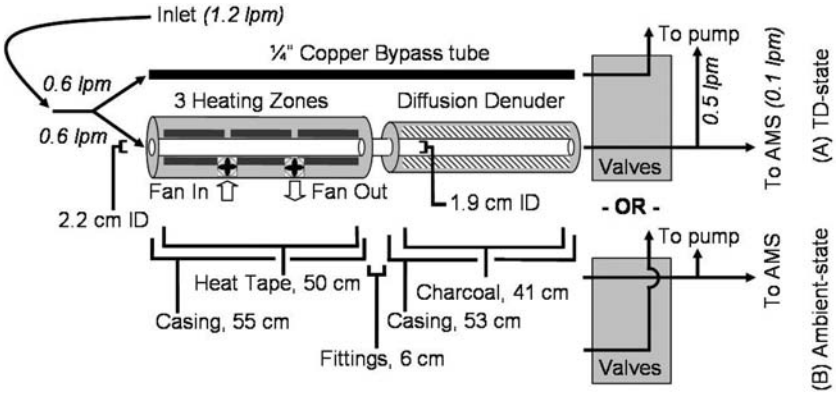


FIG. 1. Schematic diagram for thermodenuder and typical flow paths, with flow rates through each channel, and dimensions of the unit. Valve orientation for TD-state and ambient-state are both shown.

were recently pointed out as a problem in some previous studies by An et al. (2007). These authors studied the effect of residence time in the heating section of the TD and concluded that the RT of 1.6 s used by Kalberer et al. (2004) and Baltensperger et al. (2005) was too short and may have resulted in some biases in their analyses. With an ambient PFRT ∼21 s our TD is close to the PFRT of 31 s (15.8 s centerline RT) used by An et al. and should avoid major kinetic limitations.

The AMS has a total particle collection efficiency (CE) that is a combination of CE values due to transmission through the lens and inlet system, size- and shape-dependent losses, and particle bounce from the vaporizer (Huffman et al. 2005). Decreased collection efficiency due to shape-dependent losses ($E_s$) has been shown to be unimportant in multiple field campaigns (i.e., $E_s \sim 1$) (Huffman et al. 2005; Salcedo et al. 2007). The collection efficiency due to bounce ($E_b$) dominates total CE for particle sizes that the aerodynamic lens allows to pass efficiently, causing CE to remain remarkably constant at approximately 50% during most ambient campaigns (Alfarra et al. 2004; Canagaratna et al. 2007; Drewnick et al. 2004; Zhang et al. 2004), although it has known deviations from this value for some extremes of phase and composition, e.g., for very acidic particles (Quinn et al. 2006). If $E_b$ decreased after evaporation of some of the particle material in the TD as more of the solid, less-volatile material remained behind, the apparent volatility reported by the TD-AMS measurements would be higher than the real volatility. It is also possible in principle that $E_s$ could be reduced after the TD if some particles crystallized into very non-spherical shapes upon heating, which would lead to a similar effect.

## RESULTS AND DISCUSSION

### Temperature Profile Characterization

The newly designed TD was first characterized in the laboratory prior to field experimentation. Faulhaber et al. (2007) discusses the technique by which data from this TD design can provide species vapor pressure (or vapor pressure distribution). This was achieved by empirically calibrating the instrument for species of known vapor pressures and determining a relationship between these vapor pressures and their characteristic evaporation temperatures in the TD, which can then be applied to unknown aerosol as well. Here we focus on the characterization of the temperature profile and temperature dependent particle losses in the TD.

The internal temperature profile was measured with a fiberglass-wrapped thin-wire thermocouple introduced through the middle of a 0.25 inch (0.6 cm) stainless steel tube from the front end of the TD, which protruded from the end of the tube by approximately 2 cm. The probe was held in place in the middle of the heating stage tube by use of metal clips attached to the outside of the 0.25 inch (0.6 cm) tube. Temperatures were recorded at points in the longitudinal dimension while flowing the standard flow rate of 0.6 lpm and are plotted in Figure 2. The temperature profiles show a flat region in the middle at all temperatures, with no hot or cold spots. The distance (and associated RT) along the inside of the heated tube showing a region of temperature stability (±6.5% or 15°C of the average temperature at the hottest set-point) is approximately 1.8 cm longer than shown by Wehner et al. and 7.8 cm longer than Burtscher et al. The temperatures inside the heated tube are approximately 17% in °C higher than those measured by the thermocouples that drive the temperature controllers (e.g., a 200°C set-point will heat the TD to 230°C) due to the location of the control thermocouples away from direct contact from the heating tapes. All temperatures reported in this paper are centerline (CL) temperatures calculated using the calibration from heater setting values recorded in the logged heater files.

### Particle Number and Mass Loss Characterization

Particle losses within the TD were characterized by two methods. The first was designed to measure the size-resolved number loss of particles within the TD due mostly to diffusion and thermophoresis. Burtscher et al. (2001) showed that sedimentation should only play a minor role for submicron particles. NaCl (99.0%, Sigma-Aldrich Inc.) particles were generated using a dilute (∼0.005 M) water (HPLC-grade, Burdick and Jackson) solution and TSI atomizer (Model 3076, Shoreview, MN). The resultant aerosol was dried through two diffusion driers in series, diluted with particle free air, and passed through a glass mixing volume to homogenize the particle concentration across the crosssection of the downstream tubing. Relative humidity (RH) was <15% in all cases reported here. The aerosol was then passed to a 0.25 inch (0.6 cm) Y-split tube (Brechtel Manufacturing, Hayward, CA) where one path bypasses the TD and is connected directly to the valve system (described above) and the other leads through the TD and to the valve system. The distance through the two paths between the aerosol generation system and the valves (while measuring the input aerosol) and between the exit of the TD and the valves (while measuring the TD-processed aerosol) was matched, as is done during actual operation of the system in the field, in order to measure number losses due to the TD system in a form that can be used for post-correction of field data.

A scanning mobility particle sizer (SMPS: TSI Differential Mobility Analyzer, DMA, Model 3085; TSI condensation particle counter, CPC, Model 3010) was used for particle detection. A CPC (TSI Model 3010) also sampled the flow upstream of the Y-split to monitor the total particle concentration output from the atomizer as a function of time. NaCl particles were chosen for the study of size-resolved number loss because of their ease of generation from a water solution and for their nonvolatility under all experimental temperatures. Figure 3 shows the resultant number losses. The curves at each of the three temperatures were achieved by taking the ratio of the output size distribution to the input distribution and averaging over a number of scans and experiments. Data at additional temperatures (not shown) were acquired and vary smoothly between the limits shown. Error bars are standard deviation of the data points

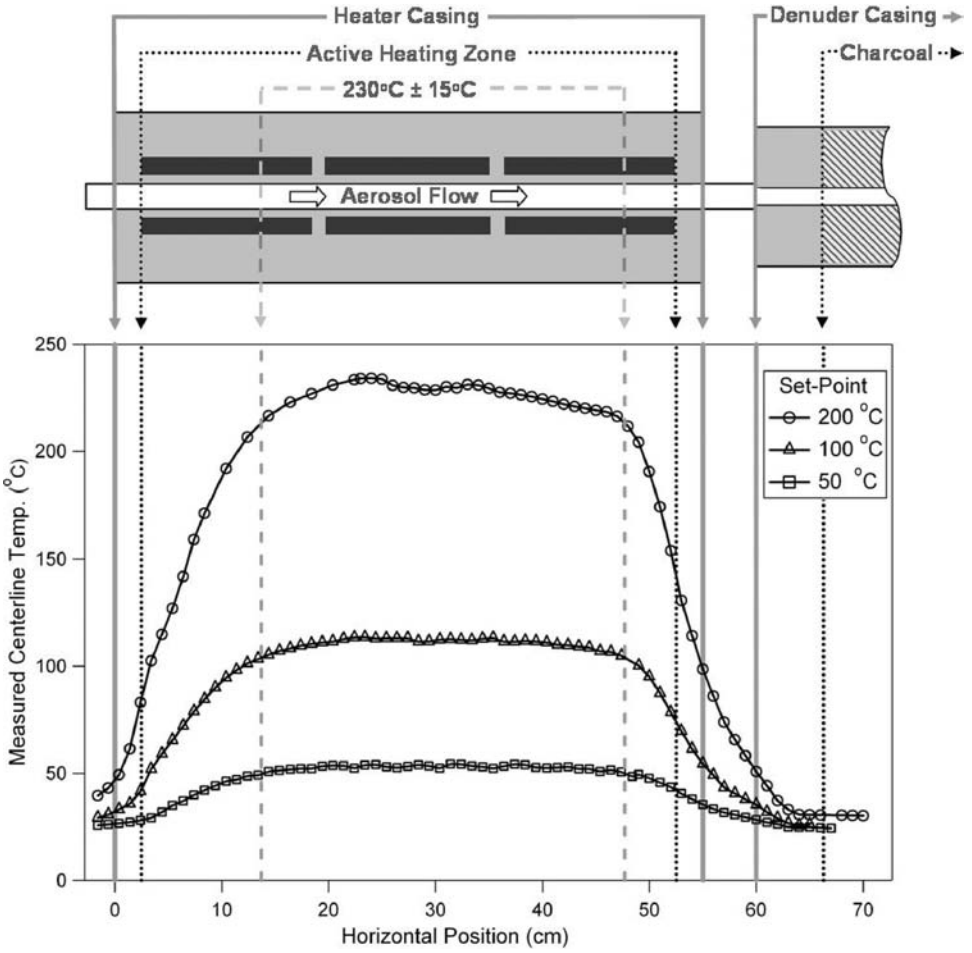


FIG. 2. Longitudinal temperature profile showing temperature at each point within the TD for the current design for three set temperatures. Schematic diagram of TD shown above graph to scale in the horizontal coordinate (but not in the vertical). Vertical arrows point to physical zones in the TD that correspond to: the outer dimensions of the physical casing, the region of active heating (where the tube is wrapped with heating tape), and the region corresponding to $T_{avg} \pm 6.5\%$ (or $\pm 15^{\circ}C$ at $230^{\circ}C$).

(shown only in a few representative regions to reduce clutter on the plot). The dotted line shows the estimated theoretical limit for diffusion loss at ambient temperature as a function of size. The loss curve at ambient temperature from Wehner et al. (2002) is also plotted to show reasonable agreement between these tests (Note: Ag particles were used in the Wehner experiment). Experimental transmission shown here is within error bars of the calculated transmission indicating no additional significant loss mechanisms exist in the system at ambient temperature. The points from Wehner et al. show higher transmission, but are also significantly above the calculated transmission, the reasons for which are unclear. The particle losses increase for smaller sizes and are approximately constant above 80 nm. The average losses for each experimental curve above 80 nm are used as the integrated number loss over the particle size range where mass is important for ambient particles (e.g., Salcedo et al. 2006). These averages are re-plotted in Figure 4 as a function of temperature. This plot shows the relationship between mass transmission in the typical ambient size range through the TD and its temperature set-point. As the TD temperature increases the particle losses increase linearly from 5% at 54°C to approximately 20% and 230°C due to additional thermophoretic forces. Thermophoresis will act to focus the particles in the heated section, but de-focus the particle stream as it enters the cooler denuding section. These increased losses at higher temperatures are expected and are within the range of characterizations carried out in previous studies of heated tubes using both theoretical (Housiadas and Drossinos 2005; Stratmann and Fissan 1988) and experimental (Burtscher et al. 2001; Tsai et al. 2004; Walsh et al. 2006) techniques. While diffusion increases greatly as particle size decreases, thermophoretic forces are not strongly size-dependent (Burtscher et al. 2001; Hinds, 1999b), but can move particles closer to the walls where diffusion of small particles can be more efficient. The inverse of the fitted line in Figure 4 can be applied to ambient data to correct for losses of mass as a function of temperature.

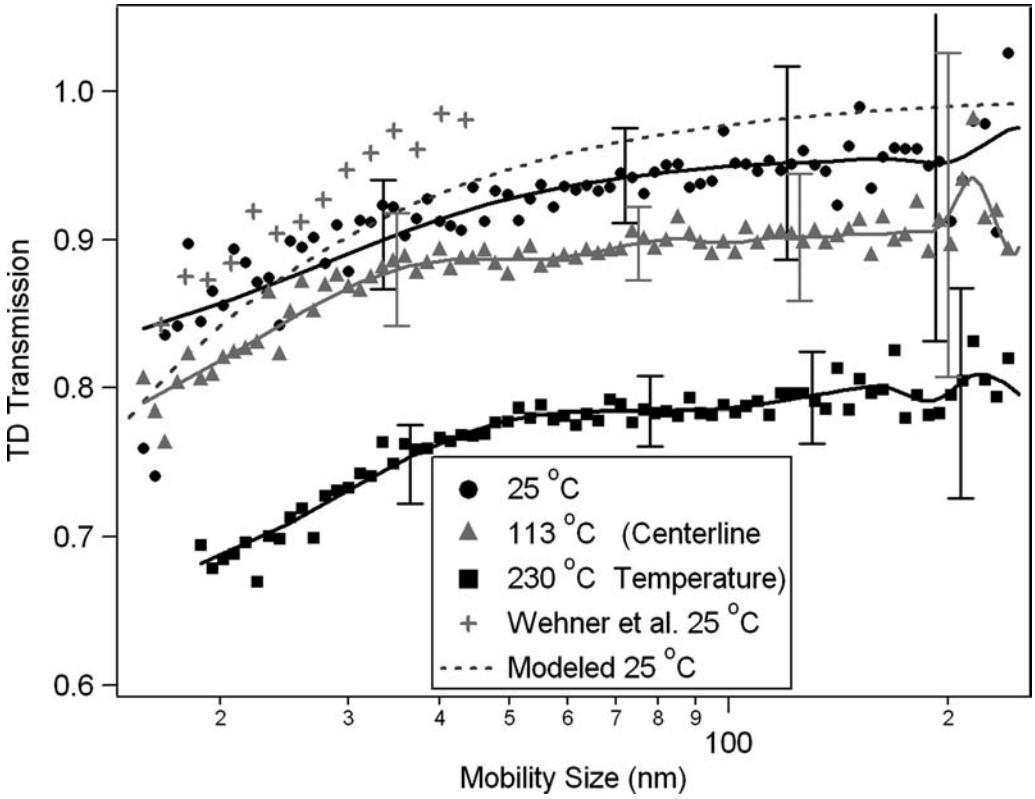


FIG. 3. Particle number loss as a function of size within the TD at three different temperatures, as due to diffusion and thermophoresis. Experimental curves at three different temperatures are shown, as well as comparisons with the theoretical diffusion limit (Cheng 2001; Hinds 1999a), and published losses from Wehner et al. (2002). Lines are spline fits to guide the eye.

Monodisperse particle number losses for species with different volatilities were also characterized. Particles were atomized and dried, as described above, and were then sent through a DMA for size-selection. Two TSI Model 3010 CPCs were placed immediately up-, and down-stream of the TD, and the respective number counts entering and exiting the TD were measured. Figure 5 shows the relationship of number loss through the TD as a function of temperature for NaCl and $(NH_4)_2SO_4$ (99.7%, Fisher Chemicals) at several sizes. The number loss curves for NaCl (Figure 5a) show no increase in particle losses as particle size decreases to 50 nm at higher temperature. The $(NH_4)_2SO_4$ curves (Figure 5b), however, show additional number losses of smaller particles after evaporation at and above 170°C as the original 50 nm size is reduced into a size range where diffusion is more efficient. Due to kinetic limitations in particle evaporation and/or small non-volatile impurities, even after most of the particle mass has evaporated at high temperatures there may still be a significant fraction of the particle number remaining which will therefore still be counted by the CPC. For example, a 200 nm particle that shrinks by a factor of 10 in diameter to 20 nm will shrink by a factor of 1000 in volume and mass. The particle will retain only 0.1% of its original mass, which is negligible from the mass perspective, but it will still be counted efficiently by the CPC. Alternatively, there may be nucleation of some particles after the evaporation of most of the sulfate material followed by cooling, creating a large number of small particles. We have so far not seen evidence of this type of nucleation on this TD system, however. A small amount of non-volatile solute

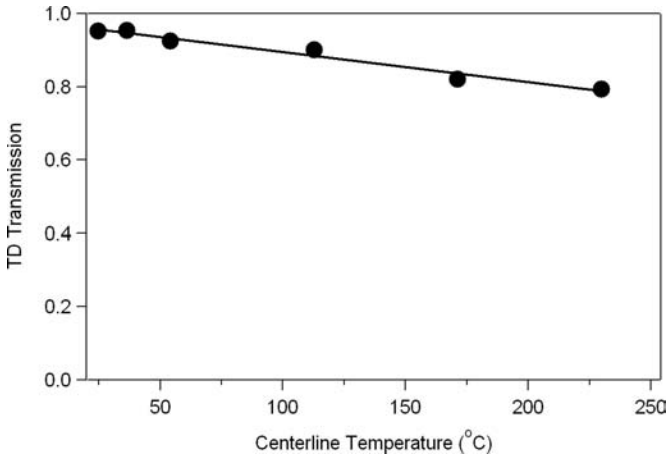


FIG. 4. Estimated particle mass loss within the TD as a function of temperature for typical submicron ambient particle distributions, shown as the integrated number loss in the particle size region where mass is important for typical ambient size distributions (above 80 nm). Line is a linear fit of $y = -0.00082 \times + 0.98$.

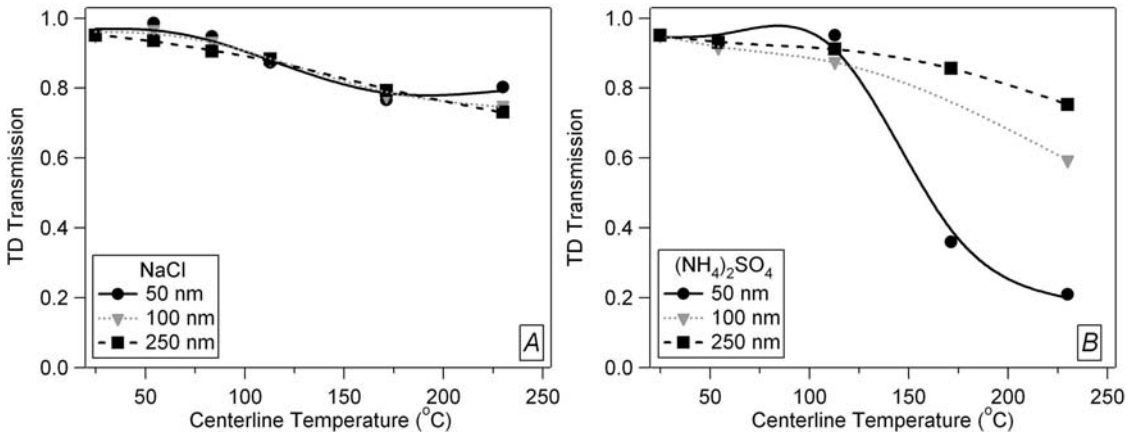


FIG. 5. Particle number loss as a function of temperature for two species, each for monodisperse sizes of 50, 100, and 250 nm. (a) NaCl, (b) $(NH_4)_2SO_4$. Data has been normalized to number losses at ambient temperature. Lines are spline fits to guide the eye.

impurity could also account for a residual core after heating, but this would again not account for significant mass. While this effect enhances the losses of smaller particles in ambient data, their contribution to the total ambient mass (and thus the positive bias on the mass loss) is small compared to larger particles.

### TD Response to Standard Chemical Species

The TD system was characterized with respect to several standard chemical species to understand their behavior as a function of TD temperature. Polydisperse particle distributions similar to typical urban atmospheric conditions were atomized, dried, and mixed with particle free air as described above. The flow system was arranged as in typical field study, with the tube distance and bends between the TD and valves, and the valves and detection instrumentation minimized. A 171 cm bypass line of 1/4″ copper tube was routed around the TD (avoiding rising hot air) to the valves. An AMS was used to detect the mass remaining after the TD, or via the bypass. The resultant volatility information for individual chemical species is most easily viewed by means of a TD "thermogram," which plots the aerosol mass fraction remaining after heating as a function of temperature. Figure 6 shows the thermograms for four standard chemical species. $NH_4NO_3$ (99.9%, Fisher Chemicals) and $NH_4Cl$ (99%, Mallinckrodt-Baker, Inc.) clearly show the highest volatility, with $(NH_4)_2SO_4$ showing intermediate volatility, and CsCl (>98%, Sigma Chemical Co.) showing virtually no evaporation with increasing temperature. CsCl was chosen because its volatility is significantly lower than $(NH_4)_2SO_4$, but high enough to evaporate on the AMS vaporizer. The thermograms for each of the other species were consistently reproducible, but the ammonium sulfate showed some variability between the curves at the 10–20% level between 90–175°C. Although the causes for this variability are not fully understood, it is possible that a change in pure ammonium sulfate particle phase (or shape) is caused by the heat in the TD, causing the AMS $E_b$ (or $E_s$) to decrease somewhat. This effect would primarily be an AMS issue and not directly related to the TD design. However, this variability is small compared to the range of volatilities measurable with the TD-AMS, as illustrated by comparison with the other 3 species in the figure.

### Automated Switching for Field Application

This thermodenuder design allows temperature-stepping in order to characterize volatility over a large temperature range and timescales of 1–3 h, short enough that under most conditions the ambient aerosol has not changed significantly. Since the AMS is a fast detector, periods of faster ambient changes can be removed from the analysis. During field sampling the flow to be analyzed is split into two parallel lines (Figure 1). One line leads

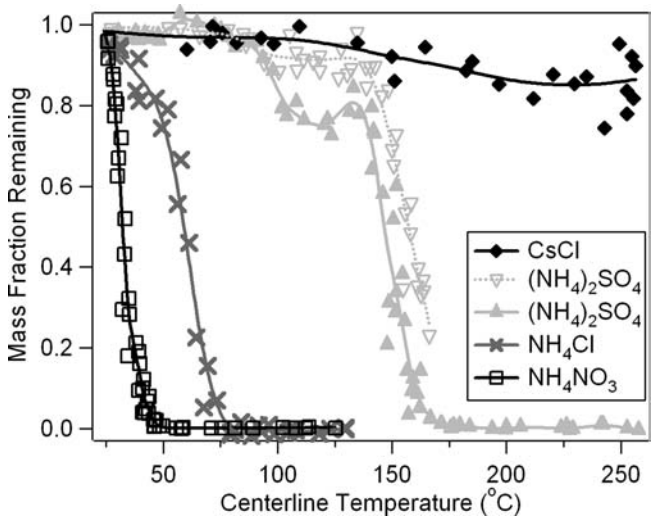


FIG. 6. Response to heating shown as a function of temperature for polydisperse species generated in the laboratory. $(NH_4)_2SO_4$ curves highlight variability while using the AMS as a particle detector. Lines are spline fits to guide the eye.

directly to the detecting instrumentation, and the second passes first through the TD and then to the same instruments. A custom valve system rapidly and automatically switches the sample that reaches the instruments between ambient (un-denuded) and thermally denuded at regular intervals (between 1 and 10 min, depending on the study). While the system is in TD-sampling state the temperature is held constant, and while the system is in ambient-sampling state the temperature is changed to another set-point. The sampling instruments detect the particle mass that has not evaporated after passing through the TD; at successively higher TD temperatures the particle mass remaining is further reduced. During standard ambient campaign operation a full cycle time of 160 minutes allows for 7 different temperature steps between 50 and 230°C, in addition to interleaved measurements at ambient T (bypassing the TD). The system has been used in several field campaigns, but examples here are shown from MILAGRO and FLAME in Figure 7. In each study, the TD was followed by a high-resolution time-of-flight AMS (HR-ToF-AMS) (DeCarlo et al. 2006). Sampling during MILAGRO (Megacity Initiative: Local And Global Research Observations) took place at the T0 Supersite inside Mexico City (north of downtown) in March 2006 (Molina et al. 2008). FLAME (Fire Lab At Missoula Experiment) took place June 2006 and 2007 at the US Forest Service Fire Sciences Lab in Missoula, MT. The FLAME study measured highly diluted (∼×10,000) smoke from open air burning of ∼15 different biomass specimens (∼200 grams each) over the course of one week. The smoke was mixed into a large chamber, and aerosol from flaming and smoldering phases of combustion was allowed to mix and reach a stable level before starting the TD-AMS cycle. More detailed analyses of the TD-AMS data from these studies are presented elsewhere (Huffman et al. 2008).

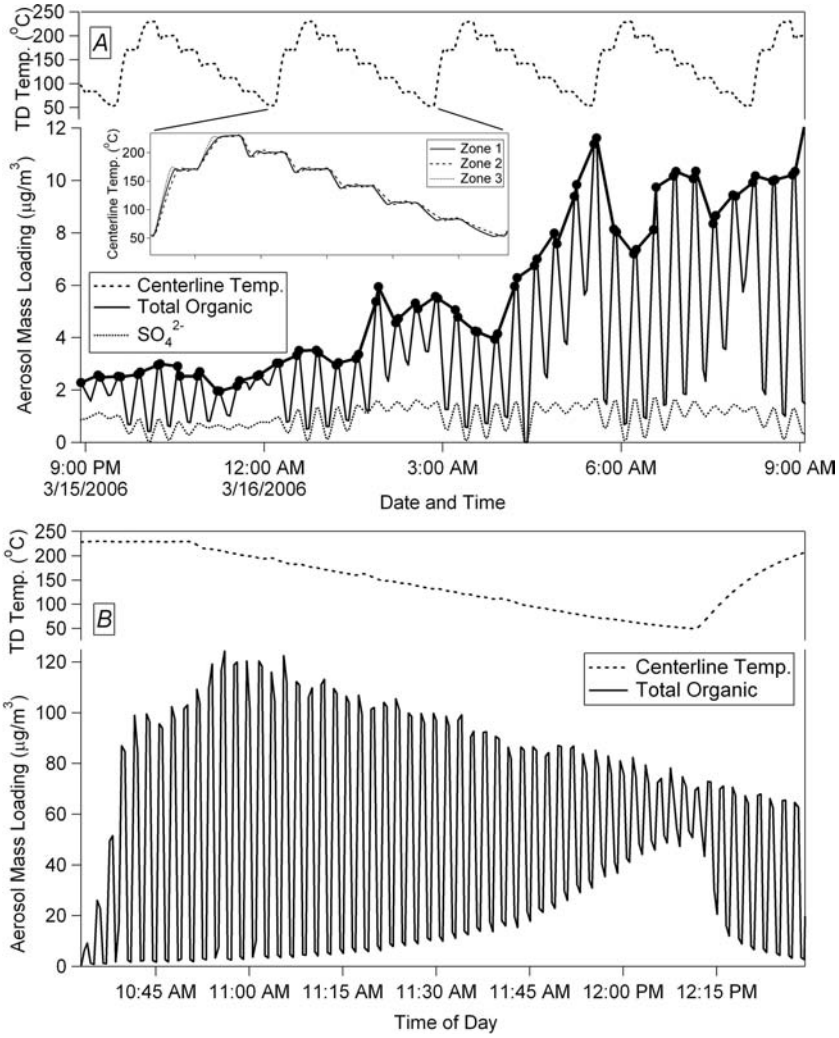


FIG. 7. Example data showing fast temperature-cycling and resultant AMS mass loadings after passing through TD. (a) Standard ambient field campaign operation with 10-minute valve switches (MILAGRO), with total organic and sulfate signals shown. (b) Modified quicker-stepping laboratory experiment operation with constantly changing TD temperature and 1-minute valve switches (FLAME).

Figure 7a shows a typical temperature program for ambient sampling at the top, and the resultant AMS data on the bottom. The thick line running through the top-most point of the total organics points is the ambient mass loading as would be measured without the use of the TD. The mass remaining after the TD is shown by the deep valleys every twenty minutes. One can see that at low temperatures the relative amount of organic aerosol mass remaining is high, while at high temperatures that amount is much lower. The temperature cycling program for the FLAME laboratory studies was optimized to achieve higher temperature resolution for shorter available total sampling times. During these experiments when the overall total aerosol mass loading (generated from burning of small amounts of biomass specimens in a large chamber) had stabilized, the temperature of the TD controller was programmed to ramp slowly from 230°C to near ambient at about 2.5°C $min^{-1}$, while the valve system switched every minute (Figure 7b). This achieves considerably higher temperature resolution of ∼5°C compared with ∼30°C for the ambient procedure in Figure 7a, however it does not allow for V/W mode switching of the HR-ToF-AMS which was required for ambient sampling.

## Field Demonstration

As an example, Figure 8a shows thermograms for MILAGRO campaign averages of sulfate, ammonium, chloride, nitrate, and organic aerosol (OA), as well as OA from Lodgepole Pine burning from the FLAME study. These data are shown to highlight the range of volatilities observed, from highly semi-volatile pine OA to much less volatile MILAGRO sulfate. The sulfate thermograms show very low volatility up to 141°C, with a sharp decrease in particle mass immediately after. The lodgepole pine OA, however, shows only 11% remaining at 141°C. Nitrate and chloride also show high volatility, consistent with their dominant non-refractory forms being ammonium nitrate and ammonium chloride as identified previously (DeCarlo et al. 2007; Salcedo et al. 2006). Chloride does show a residual at high temperatures indicating the presence of other less volatile chloride species such as zinc or lead chloride, consistent with other measurements (Moffet et al. 2007). Note that all data shown here has been corrected for experimentally determined losses, as shown in Figure 4. The sigmoidal shape of the sulfate curve points to one compound dominating the total sulfate mass (Faulhaber et al. 2007; Twomey 1968). Note also that there is a slight apparent increase in the sulfate curve at approximately 150°C. While this behavior is not completely understood, it may be related to small changes of the AMS $E_b$ after the aerosol is heated as discussed earlier. It can contribute a 10–20% variability in the sulfate mass remaining between 90–175°C, but the overall shape and 50% evaporation point remain largely unaffected. The total organic volatility shows a more gradual decrease in particle mass as a function of size, indicating a complex mixture of semivolatile OA compounds over a wide range of volatilities (Donahue et al. 2006). Figure 8b shows MILAGRO campaign-average sulfate during diurnal periods of: early morning (0–4 AM), mid-morning (5–8 AM), and mid-afternoon (1–4 PM), local time, which show little dependence of the shape of the curves on time of the day. Data from laboratory-generated ammonium sulfate (replotted from Figure 6) is also plotted in Figure 8b showing a similar evaporation temperature, but with a sharper transition. This confirms the dominant chemical form of the sulfate as ammonium sulfate, as concluded previously (DeCarlo et al. 2007; Salcedo et al. 2006).

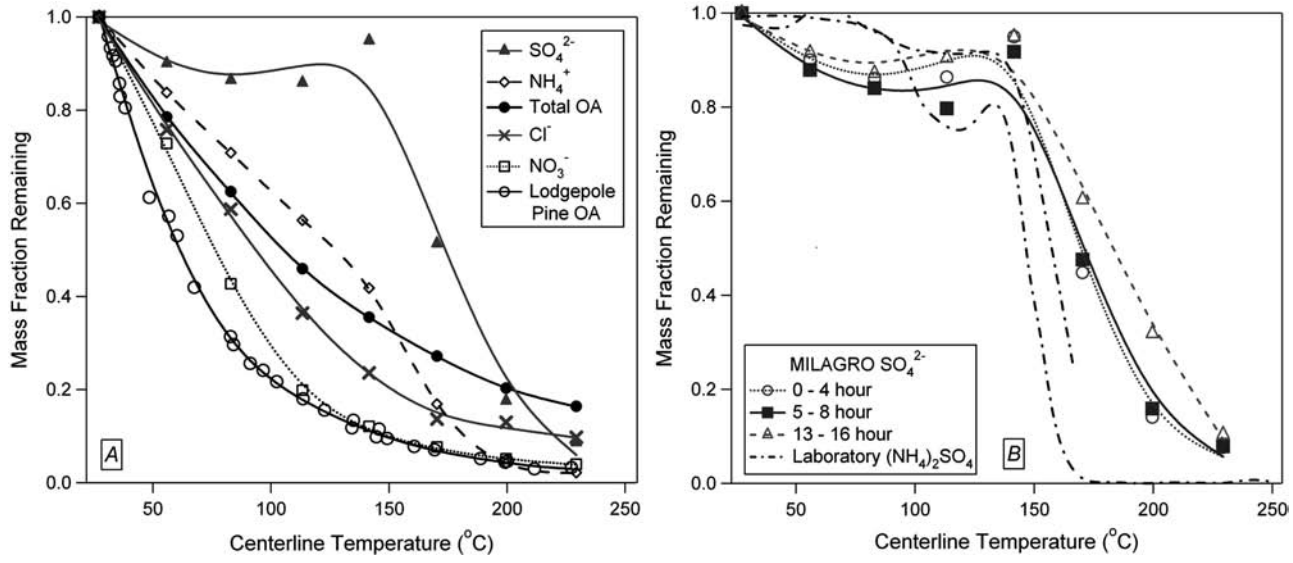


FIG. 8. Fraction of particle mass remaining after passing through TD as a function of TD temperature ("thermograms") showing range of volatilities observed. (a) MILAGRO averages for four inorganic species and Total OA, as well as Lodgepole Pine from FLAME. (b) Diurnal thermogram plots for total aerosol sulfate during MILAGRO campaign. Volatility of laboratory-generated ammonium sulfate is plotted with ambient sulfate data in panel B. Lines are spline fits to guide the eye.

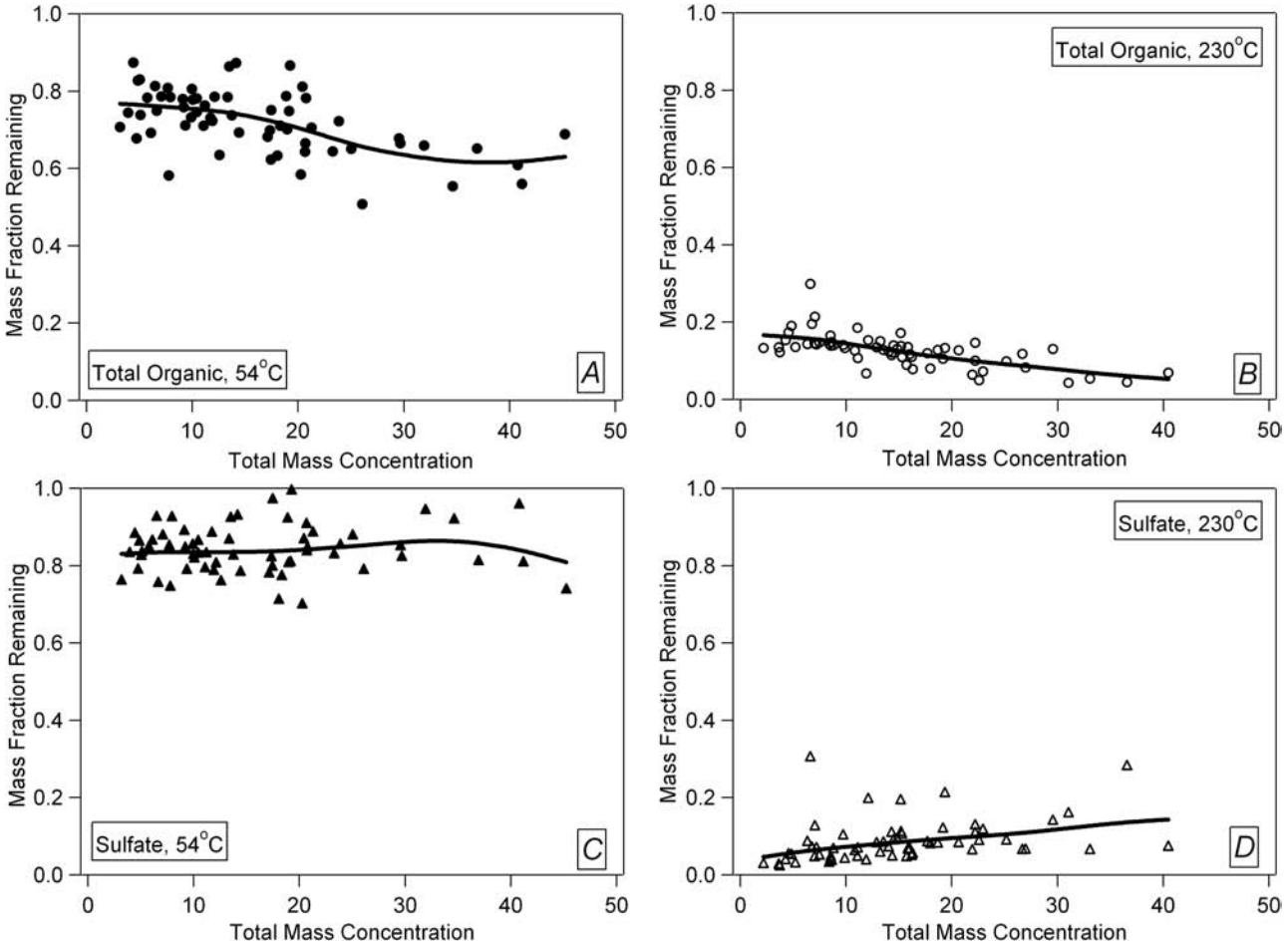


FIG. 9. Mass fraction remaining after TD plotted versus total aerosol mass concentration ($\mu$g/m$^3$) used as an estimation of gas recondensation onto remaining particles. Total organic aerosol (OA) and aerosol sulfate are each shown at the temperature bounds used in the MILAGRO study. Panels show: (a) Total OA at 54°C, (b) Total OA at 230°C, (c) sulfate at 54°C, (d) sulfate at 230°C. Lines are spline fits to guide the eye.

The thermogram (especially the sharp decrease in mass fraction remaining) is less sharp for ambient particles than for laboratory ammonium sulfate, which may be due to the internal mixing of sulfate with more volatile (such as ammonium bisulfate) or more refractory species in some particles. Additional analyses of the MILAGRO thermograms and their variability will be presented elsewhere.

### Potential Issues for TD-AMS Quantification

The TD design works under the assumption that certain particle species will evaporate in the heating stage and will be removed by diffusion to the activated carbon charcoal in the denuding phase immediately after. Implicitly this assumes that the surface area presented by the charcoal is much larger than that presented by the residual aerosol particles. The diffusion time for vapors to reach the charcoal is ~100 ms, which is short compared to the time spent in the denuding section. Recondensation of vapors on the aerosol particles has been observed in some previous studies carried out under high aerosol concentrations (Sakurai et al. 2003). Recondensation is likely a larger issue for TD designs without an adsorbent section, but less important in VTDMAs due to the low particle surface area present after size selection. The effect of recondensation will lead to an underestimation of particle volatility. Recondensation can be post-diagnosed (and partially corrected for) by analyzing the thermograms vs. aerosol surface area (SA) concentration after the TD, as recondensation will be larger when the ratio of aerosol to adsorbent surface area is higher. Figure 9 shows the fraction of particle mass remaining after the TD as a function of the total ambient particle mass (used as a surrogate for total particle SA since the particle size distribution is relatively constant (Salcedo et al. 2006)) during MILAGRO for total organics and sulfate at 54 and 230°C each. The slope of the first three panels is either approximately zero or slightly negative, thus showing no signs of recondensation. The plot for sulfate at 230°C, however, does show some potential evidence of recondensation. Ammonium sulfate has the lowest vapor pressure of the major species

detected by the AMS, and as temperature decreases in the cooling region these molecules may efficiently recondense onto the surface of a nearby particle (uptake coefficient $\gamma \sim 1$) before they have had time to reach the charcoal adsorbent. This phenomenon was also observed for sulfate at 200°C (not shown). Since the sulfate size distributions were similar at the different concentration levels, the effect discussed here is likely not related to reduced evaporation at high concentrations. This latter effect may be important in some cases. Overall this qualitative analysis suggests that recondensation is typically not a large problem for our TD under the relatively high ambient concentrations of Mexico City, and its effects can be diagnosed with the analysis technique just described.

The ambient data analyzed so far indicate that the effect of varying $E_b$ (or $E_s$), if present, is small. For example, qualitative difference in thermograms in Figure 8 for the total organics and sulfate indicates that the chemical difference in volatility is indeed the most significant factor for the appearance of the curves; i.e., if changes in $E_b$ were the dominant mechanism leading to the observed thermograms in the TD-AMS system, the sulfate and organic thermograms would be very similar, given that much of the sulfate and organic mass is in aged internally mixed particles in Mexico City (Salcedo et al. 2006). The difference between these curves, as well as the similarity of the sulfate thermograms to the laboratory data indicate strongly that, while changes in $E_b$ may be a contributing factor in the shape of the curves, the dominant effect of the technique is volatility separation. As discussed previously, $E_b$ change may play a role at a 10–20% level for sulfate between 90–175°C. Future studies should address this question by directly comparing $E_b$ and $E_s$ in the AMS using the internal light scattering unit (Cross et al. 2007) and beam width probe (Huffman et al. 2005) for ambient particles that have gone through and bypassed the TD.

It should also be noted that the use of the charcoal denuder, while necessary to strip volatilized material away from the particles when mass concentrations are high, can also cause particle evaporation not due directly by increased temperature. In other words, semivolatile species which have a significant fraction of their concentration in the gas-phase in equilibrium may partially evaporate as the gas-phase is denuded at ambient temperature without and heating. This will be seen by unreasonably high volatility at ambient temperature, and while rare, we have qualitatively observed it during some very high concentration experiments (fresh diesel exhaust sampled under low dilution). The denuder section filled with fresh charcoal also appeared to strip material from laboratory-generated pure ammonium nitrate aerosol at ambient temperature. This effect disappeared after conditioning the charcoal by flowing air with ammonia (generated by passing the incoming air over an ammonia solution) through the TD for a short period. We did not observe changes on the ammonium nitrate evaporation curve with time in ambient studies, which would have suggested variation on this effect with time.

## CONCLUSIONS

We have built upon the thermodenuder designs of Wehner et al. (2002) and Burtscher et al. (2001) to develop a technique to quickly measure chemically-resolved ambient aerosol volatility in the field for the first time. The TD design presented here has been optimized to reduce thermal mass and implement rapid temperature control, and a computer-controlled valve system has been designed to achieve fast ambient/TD switching. The longitudinal temperature profiles are comparable to the previous designs. Particle number losses were characterized experimentally as a function of size and TD temperature and are also close to both calculated losses and those from previous studies. The total mass loss for typical ambient submicron particle size distributions was estimated to increase from approximately 5% at 54°C to 20% at 230°C. These additional losses are mostly due to thermophoretic forces at the boundary of the heating stage to the cooling stage and are within experimental and calculated losses for other similar systems. The TD response to lab-generated chemical species was also characterized. Example ambient data are presented in which the volatility of the different species varies as expected. Positive artifacts due to gas recondensation can be a potential problem for TD measurements, but are significantly reduced by the addition of a charcoal diffusion denuder. The effect has been investigated for operation in the field and is both small and diagnosable (potentially post-correctable). Variations in AMS collection efficiency after the TD may be responsible for thermogram variations of the order of 10–20% for sulfate between ∼90–175°C. Further design improvements are needed to further flatten the longitudinal temperature profile at the beginning and end of the heated zone and minimize thermophoretic losses and effects, especially at the transition between the heating and cooling sections. It may be possible to change temperatures more rapidly, but this may require a more complex control system and/or active cooling to allow the temperature to stabilize before the next data point. Adding more heating control sections (for example, from three used here to five, each with shorter sections and more concentrated power capacity per unit length of the TD at the entrance and exit) would help achieve this objective and thus provide a longer residence time near the temperature set-point in the heated section.

## REFERENCES

Alfarra, M. R., Coe, H., Allan, J. D., Bower, K. N., Boudries, H., Canagaratna, M., Jimenez, J., Jayne, J., Garforth, A., Li, S. M., and Worsnop, D. (2004). Characterization of Urban and Rural Organic Particulate In the Lower Fraser Valley Using Two Aerodyne Aerosol Mass Spectrometers, *Atmos. Environ.* 38:5745–5758.

An, W. J., Pathak, R. K., Lee, B. H., and Pandis, S. N. (2007). Aerosol Volatility Measurement Using an Improved Thermodenuder: Application to Secondary Organic Aerosol, *J. Aerosol Sci.* 38:305–314.

Baltensperger, U., Kalberer, M, Dommen, J., Paulsen, D., Alfarra, M. R., Coe, R., Fisseha, H., Gascho, R. A., Gysel, M., Nyeki, S., Sax, M., Steinbacher, M., Prevot, A. S. H., Sjogren, S., Weingartner, E., and Zenobi, R. (2005). Secondary Organic Aerosols from Anthropogenic and Biogenic Precursors, *Faraday Discussions* 130:265–278.

Brooks, B. J., Smith, M. H., Hill, M. K., and O'Dowd, C. D. (2002). Size-Differentiated Volatility Analysis of Internally Mixed Laboratory-Generated Aerosol, *J. Aerosol Sci.* 33:555–579.

Burtscher, H., Baltensperger, U., Bukowiecki, N., Cohn, P., Huglin, C., Mohr, M., Matter, U., Nyeki, S., Schmatloch, V., Streit, N., and Weingartner, E. (2001). Separation of Volatile and Non-Volatile Aerosol Fractions by Thermodesorption: Instrumental Development and Applications, *J. Aerosol Sci.* 32:427–442.

Canagaratna, M. R., Jayne, J. T., Jimenez, J. L., Allan, J. D., Alfarra, M. R., Zhang, Q., Onasch, T. B., Drewnick, F., Coe, H., Middlebrook, A., Delia, A., Williams, L. R., Trimborn, A. M., Northway, M. J., DeCarlo, D. F., Kolb, C. E., Davidovits, P., and Worsnop, D. R. (2007). Chemical and Microphysical Characterization of Ambient Aerosols with the Aerodyne Aerosol Mass Spectrometer, *Mass Spectrom. Rev.* 26:185–222.

Cheng, Y.-S. (2001). Condensation Detection and Diffusion Size Separation Techniques, in *Aerosol Measurement: Principles, Techniques, and Applications*, P. A. Baron and K. Willeke, John Wiley & Sons, Inc.

Clarke, A. D. (1991). A Thermo Optic Technique for Insitu Analysis of Size-Resolved Aerosol Physicochemistry, *Atmos. Environ. Part a-General Topics*, 25:635–644.

Cobourn, W. G., Husar, J. D., Husar, R. B., and Kohli, S. (1981). Airborne In-Situ Measurement of Paticulate Sulfur and Sulfuric Acid with Flame Photometry and Thermal Analysis, *Atmos. Environ.* 15:2565–2571.

Cross, E. S., Slowik, J. G., Davidovits, P., Allan, J. D., Worsnop, D. R., Jayne, J. T., Lewis, D. K., Canagaratna, M., and Onasch, T. B. (2007). Laboratory and Ambient Particle Density Determinations using Light Scattering in Conjunction with Aerosol Mass Spectrometry, *Aerosol Sci. Technol.* 41:343–359.

Daly, G. L., and Wania, F. (2004). Simulating the Influence of Snow on the Fate of Organic Compounds, *Environ. Sci. Technol.* 38:4176–4186.

Davidson, C. I., Phalen, R. F., and Solomon, P. A. (2005). Airborne particulate matter and human health: A review, *Aerosol Sci. Technol.* 39:737–749.

DeCarlo, P. F., Dunlea, E. J., Kimmel, J. R., Aiken, A. C., Sueper, D., Crounse, J., Wennberg, P. O., Emmons, L., Shinozuka, Y., Clarke, A. D., Zhou, J., Tomlinson, J., Collins, D., Knapp, D., Weinheimer, A., Campos, T., and Jimenez, J. L. (2007). Fast Airborne Aerosol Size and Chemistry Measurements with the High Resolution Aerosol Mass Spectrometer during the MILAGRO Campaign, *Atmos. Chem. Phys. Discuss.* 7:18269–18317.

DeCarlo, P. F., Kimmel, J. R., Trimborn, A., Northway, M. J., Jayne, J. T., Aiken, A. C., Gonin, M., Fuhrer, K., Horvath, T., Docherty, K. S., Worsnop, D. R., and Jimenez, J. L. (2006). Field-Deployable, High-Resolution, Time-of-Flight Aerosol Mass Spectrometer, *Anal. Chem.* 78:8281–8289.

Dinger, J. E., Howell, H. B., and Wojciech, Ta (1970). On Source and Composition of Cloud Nuclei in a Subsident Air Mass over North Atlantic, *J. Atmos. Sci.* 27:791–797.

Donahue, N. M., Robinson, A. L., Stanier, C. O., and Pandis, S. N. (2006). Coupled Partitioning, Dilution, and Chemical Aging of Semivolatile Organics, *Environmental Science & Technology* 40:2635–2643.

Drewnick, F., Schwab, J. J., Jayne, J. T., Canagaratna, M., Worsnop, D. R., and Demerjian, K. L. (2004). Measurement of Ambient Aerosol Composition During the PMTACSNY 2001 using an Aerosol Mass Spectrometer. Part I: Mass concentrations, *Aerosol Sci. Technol.* 38:92–103.

Ehn, M., Petaja, T., Birmili, W., Junninen, H., Aalto, P., and Kulmala, M. (2007). Nonvolatile Residuals of Newly Formed Atmospheric Particles in the Boreal Forest, *Atmospheric Chemistry and Physics*, *7*:677–684.

Faulhaber, A., Klingbeil, B. M., Jimenez, J. L., Jayne, J. T., Worsnop, D. R., and Ziemann, P. J. (2008). Characterization of a Thermodenuder-Particle Beam Mass Spectrometer System for the Study of Organic Aerosol Volatility and Composition, *Aerosol Science and Technology, In Preparation.*

Franz, T. P., Eisenreich, S. J., and Holsen, T. M. (1998). Dry Deposition of Particulate Polychlorinated Biphenyls and Polycyclic Aromatic Hydrocarbons to Lake Michigan, *Environ. Sci. Technol.* 32:3681–3688.

Goetz, A., Preining, O., and K. T. (1961). The Metastability of Natural and Urban Aerosols, *Pure and Applied Geophysics* 50:67–80. 39.

Hinds, W. C. (1999a). Brownian Motion and Diffusion, in *Aerosol Technology: Properties, Behavior, and Measurement of Airborne Particles*, John Wiley & Sons, Inc. 150–170.

Hinds, W. C. (1999b). Thermal and Radiometric Forces, in *Aerosol Technology: Properties, Behavior, and Measurement of Airborne Particles*, John Wiley & Sons, Inc. 171–181.

Hoppel, W. A., Dinger, J. E., and Ruskin, R. E. (1973). Vertical Profiles of CCN at Various Geographical Locations, *Journal of the Atmospheric Sciences*, 30:1410-1420.

Housiadas, C., and Drossinos, Y. (2005). Thermophoretic Deposition in Tube Flow, *Aerosol Sci. Technol.* 39:304–318.

Hudson, J. G., and Da, X. Y. (1996). Volatility and Size of Cloud Condensation Nuclei, *J. Geophys. Res.-Atmospheres*, 101:4435–4442.

Huffman, J. A., Aiken, A. C., Docherty, K., Ulbrich, I. M., Decarlo, P., Jayne, J. T., Onasch, T. B., Trimborn, A., Worsnop, D. R., Ziemann, P. J., and Jimenez, J. L. (2008). Volatility of Primary and Secondary Organic Aerosols in the Field Contradicts Current Model Representations, *Submitted April 2008*.

Huffman, J. A., Jayne J. T., Drewnick F. , Aiken A. C., Onasch T., Worsnop D. R., and Jimenez, J. L. (2005). Design, Modeling, Optimization, and Experimental Tests of a Particle Beam Width Probe for the Aerodyne Aerosol Mass Spectrometer, *Aerosol Science and Technology*, 39:1143–1163.

Husar, R. B., and Shu, W. R. (1975). Thermal Analyses of Los-Angeles Smog Aerosol, *J. Appl. Meteorol.* 14:1558–1565.

IPCC (2007). *Climate Change 2007*, Fourth Assesment Report, Working Group reports I to III, IPCC, Cambridge University Press, Cambridge.

Jayne, J. T., Leard, D. C., Zhang, X. F., Davidovits, P., Smith, K. A., Kolb, C. E., and Worsnop, D. R. (2000). Development of an Aerosol Mass Spectrometer for Size and Composition Analysis of Submicron Particles, *Aerosol Sci. Technol.* 33:49–70.

Jennings, S. G., and O'Dowd, C. D. (1990). Volatility of Aerosol at Mace Head, on the West-Coast of Ireland, *J. Geophys. Res.-Atmospheres*, 95:13937–13948.

Jennings, S. G., O'Dowd, C. D., Cooke, W. F., Sheridan, P. J., and Cachier, H. (1994). Volatility of Elemental Carbon, *Geophys. Res. Lett.* 21:1719–1722.

Jimenez, J. L., Jayne, J. T., Shi, Q., Kolb, C. E., Worsnop, D. R., Yourshaw, I., Seinfeld, J. H., Flagan, R. C., Zhang, X. F. , Smith, K. A., Morris J. W., and Davidovits, P. (2003). Ambient Aerosol Sampling using the Aerodyne Aerosol Mass Spectrometer, *Journal of Geophysical Research-Atmospheres* 108:8425.

Jonsson, A. M., Hallquist, M., and Saathoff, H. (2007). Volatility of Secondary Organic Aerosols from the Ozone Initiated Oxidation of Alpha-Pinene and Limonene, *J. Aerosol Sci.* 38:843–852.

Kalberer, M., Paulsen, D., Sax, M., Steinbacher, M., Dommen J., Prevot, A. S. H., Fisseha, R., Weingartner, E., Frankevich, V., Zenobi, R., and Baltensperger, U. (2004). Identification of Polymers as Major Components of Atmospheric Organic Aerosols, *Science*, 303:1659–1662.

Kanakidou, M., Seinfeld, J. H., Pandis, S. N., Barnes, I., Dentener, F. J., Facchini, M. C., Van Dingenen, R., Ervens, B., Nenes, A., Nielsen, C. J., Swietlicki, E., Putaud, J. P., Balkanski, Y., Fuzzi, S., Horth, J., Moortgat, G. K., Winterhalter, R., Myhre, C. E. L., Tsigaridis, K., Vignati, E., Stephanou, E. G., and Wilson, J. (2005). Organic Aerosol and Global Climate Modelling: a Review, *Atmospheric Chemistry and Physics* 5:1053–1123.

Kreidenweis, S. M., McInnes, L. M., and Brechtel, F. J. (1998). Observations of Aerosol Volatility and Elemental Composition at Macquarie Island during the First Aerosol Characterization Experiment (ACE 1). *J. Geophys. Res.-Atmospheres*, 103:16511–16524.

Kuhn, T., Krudysz, M., Zhu, Y. F., Fine, P. M., Hinds, W. C., Froines, J., and Sioutas, C. (2005). Volatility of Indoor and Outdoor Ultrafine Particulate Matter near a Freeway, *J. Aerosol Sci.* 36:291–302.

Larson, T. V., Ahlquist, N. C., Weiss, R. E., Covert, D. S., and Waggoner, A. P. (1982). Chemical Speciation of H2SO4 - $(NH_4)_2SO_4$ Particles Using Temperature and Humidity Controlled Nephelometry, *Atmos. Environ. 16*:1587–1590.

Likens, G. E., Driscoll, C. T., and Buso, D. C. (1996). Long-term effects of acid rain: Response and recovery of a forest ecosystem, *Science*, 272:244–246.

Lipsky, E. M., and Robinson, A. L. (2006). Effects of Dilution on Fine Particle Mass and Partitioning of Semivolatile Organics in Diesel Exhaust and Wood Smoke, *Environ. Sci. Technol.* 40:155–162.

McMurry, P. H. (2000). A Review of Atmospheric Aerosol Measurements, *Atmospheric Environment* 34:1959–1999.

Meyer, M. B., Patashnick, H., Ambs, J. L., and Rupprecht, E. (2000). Development of a Sample Equilibration System for the TEOM Continuous PM Monitor, *Journal of the Air & Waste Management Association*, 50:1345–1349.

Moffet, R. C., de Foy, B., Molina, L. T., Molina, M. J., and Prather, K. A. (2007). Measurement of Ambient Aerosols in Northern Mexico City by Single Particle Mass Spectrometry, *Atmos. Chem. Phys. Discuss.* 7:6413–6457.

Molina, L. T., Madronich, S., Gaffney, J. S., et al. (2008). An Overview of the MILAGRO Campaign: Mexico City Emissions and Their Evolution, *In Preparation*.

Offenberg, J. H., Kleindienst, T. E., Jaoui, M., Lewandowski, M., and Edney, E. O. (2006). Thermal Properties of Secondary Organic Aerosols, *Geophys. Res. Lett.* 33:L03816.

Orsini, D. A., Wiedensohler, A., Stratmann, F., and Covert, D. S. (1999). A New Volatility Tandem Differential Mobility Analyzer to Measure the Volatile Sulfuric Acid Aerosol Fraction, *J. Atmos. Oceanic Technol.* 16:760–772.

Paulsen, D., Weingartner, E., Alfarra, M. R., and Baltensperger, U. (2006). Volatility Measurements of Photochemically and Nebulizer-Generated Organic Aerosol Particles, *J. Aerosol Sci.* 37:1025–1051. D23

Philippin, S., Wiedensohler, A., and Stratmann, F. (2004). Measurements of Non-Volatile Fractions of Pollution Aerosols with an Eight-Tube volatility Tandem Differential Mobility Analyzer (VTDMA-8), *J. Aerosol Sci.* 35:185–203.

Pinnick, R. G., Jennings, S. G., and Fernandez, G. (1987). Volatility of Aerosols in the Arid Southwestern United-States, *J. Atmos. Sci.* 44:562–576.

Pueschel, R. F., Bodhaine, B. A., and Mendonca, B. G. (1973). The Proportion of Volatile Aerosols on the Island of Hawaii, *J. Appl. Meteorol.* 12:308–315.

Quinn, P. K., Bates, T. S., Coffman, D., Onasch, T. B., Worsnop, D. R., Baynard, T., de Gouw, J. A., Golden, P. D., Kuster, W. C. Williams, E., Roberts, J. M., Lerner, B., Stohl, A., Pettersson, A., and Lovejoy, E. R.(2006). Impacts of Sources and Aging on Submicrometer Aerosol Properties in the Maine Boundary Layer Across the Gulf of Maine, *J. Geophys. Res.* 111:D23S36.

Rosen, J. M. (1971). The Boiling Point of Stratospheric Aerosols, *J. Appl. Meteorol.* 10:1044–1046.

Sakurai, H., Park, K., McMurry, P. H., Zarling, D. D., Kittelson D. B., and Ziemann, P. J. (2003). Size-Dependent Mixing Characteristics of Volatile and Nonvolatile Components in Diesel Exhaust Aerosols, *Environ. Sci. Technol.* 37:5487–5495.

Salcedo, D., Onasch, T. B., Canagaratna, M. R., Dzepina, K., Huffman, J. A., Jayne, J. T., Worsnop, D. R., Kolb, C. E., Weimer, S., Drewnick, F., Allan, J. D., Delia, A. E., and Jimenez, J. L. (2007). Technical Note: Use of a Beam Width Probe in an Aerosol Mass Spectrometer to Monitor Particle Collection Efficiency in the Field, *Atmos. Chem. Phys.* 7:549–556.

Salcedo, D., Onasch, T. B., Dzepina, K., Canagaratna, M. R., Zhang, Q., Huffman, J. A., DeCarlo, P. F., Jayne, J. T., Mortimer, P., Worsnop, D. R., Kolb, C. E., Johnson, K. S., Zuberi, B., Marr, L. C., Volkamer, R., Molina, L. T., Molina, M. J., Cardenas, B., Bernabe, R. M., Marquez, C., Gaffney, J. S., Marley, N. A., Laskin, A., Shutthanandan, V., Xie, Y., Brune, W., Lesher, R., Shirley, T., and Jimenez, J. L. (2006). Characterization of Ambient Aerosols in Mexico City During the MCMA-2003 Campaign with Aerosol Mass Spectrometry: Results from the CENICA Supersite, *Atmos. Chem. Phys.* 6:925–946.

Schneider, J., Hock, N., Weimer, S., and Borrmann, S. (2005). Nucleation Particles in Diesel Exhaust: Composition Inferred from in Situ mass Spectrometric Analysis, *Environ. Sci. Technol.* 39:6153–6161.

Shrivastava, M. K., Lipsky, E. M., Stanier, C. O., and Robinson, A. L. (2006). Modeling Semivolatile Organic Aerosol Mass Emissions from Combustion Systems, *Environmental Science & Technology* 40:2671–2677.

Simcik, M. F., Franz, T. P., Zhang, H. X., and Eisenreich, S. J. (1998). Gas-Particle Partitioning of PCBs and PAHs in the Chicago Urban and Adjacent Coastal Atmosphere: States of Equilibrium, *Environ. Sci. Technol.* 32:251–257.

Smith, M. H., and O'Dowd, C. D. (1996). Observations of Accumulation Mode Aerosol Composition and Soot Carbon Concentrations by Means of a High-Temperature Volatility Technique, *J. Geophys. Res. -Atmospheres*, 101:19583–19591.

Stanier, C. O., Pathak, R. K., and Pandis, S. N. (2007). Measurements of the Volatility of Aerosols from $\alpha$-Pinene Ozonolysis, *Environ. Sci. Technol.* 41:2756–2763.

Stratmann, F., and Fissan, H. (1988). Convection, Diffusion and Thermophoresis in Cooled Laminar Tube Flow, *J. Aerosol Sci.* 19: 793–796.

Tanner, R. L., D'Ottavio, T., Garber R., and Newman, L. (1980). Determination of Ambient Aerosol Sulfur Using a Continuous Flame Photometric Detection System. I. Sampling System for Aerosol Sulfate and Sulfuric Acid, *Atmos. Environ.* 14:121–127.

Ten Brink, H. M., Veefkind, J. P., WaijersIjpelaan, A., and vanderHage, J. C. (1996). Aerosol light-scattering in The Netherlands, *Atmos. Environ.* 30:4251–4261.

Tsai, C. J., Lin, J. S., Aggarwal, S. G., and Chen, D. R. (2004). Thermophoretic deposition of particles in laminar and turbulent tube flows, *Aerosol Sci. Technol.* 38:131–139.

Twomey, S. (1968). On the composition of cloud nuclei in the northeastern United States, *Journal de Recherches Atmospheriques*, 3:281–285.

Twomey, S. (1971a). The Composition of Cloud Nuclei, *Journal of the Atmospheric Sciences*, 28:377–381.

Twomey, S. (1971b). The Evaporation of Submicron Aerosol Particles, *Journal de Recherches Atmospheriques*, 5:93–99.

Villani, P., Picard, D., Marchand, N., and Laj, P. (2007). Design and Validation of a 6- Volatility Tandem Differential Mobility Analyzer (VTDMA). *Aerosol Sci. Technol.* 41:898–906.

Walsh, J. K., Weimer, A. W., and Hrenya, C. M. (2006). Thermophoretic Deposition of Aerosol Particles in Laminar Tube Flow with Mixed Convection, *J. Aerosol Sci.* 37:715–734.

Watson, J. G. (2002). Visibility: Science and Regulation, *J. Air & Waste Manage. Assoc.* 52:628–713.

Wehner, B., Petaja, T. Boy, M., Engler, C., Birmili, W., Tuch, T., Wiedensohler, A., and Kulmala, M. (2005). The Contribution of Sulfuric Acid and Non-Volatile Compounds on the Growth of Freshly Formed Atmospheric Aerosols, *Geophys. Res. Lett.* 32:L17810.

Wehner, B., Philippin, S., and Wiedensohler, A. (2002). Design and Calibration of a Thermodenuder with an Improved Heating Unit to Measure the Size-Dependent Volatile Fraction of Aerosol Particles, *J. Aerosol Sci.* 33:1087–1093.

Wehner, B., Philippin, S., Wiedensohler, A., Scheer, V., and Vogt, R. (2004). Variability of non-volatile fractions of atmospheric aerosol particles with traffic influence, *Atmos. Environ.* 38:6081–6090.

Went, F. W. (1960). Blue Hazes in the Atmosphere, *Nature*, 187:641–643.

Wilson, J. C., and Seebaugh, W. R. (2001). Chapter 30: Measurement of Aerosol from Aircraft, in *Aerosol Measurement: Principles, Techniques, and Applications*, P. A. Baron and K. Willeke, ed., Wiley-Interscience 894.

Zhang, Q., Canagaratna, M. Jayne, J., Worsnop, D., and Jimenez, J. (2004). Time and Size- Resolved Chemical Composition of Submicron Particles in Pittsburgh - Implications for Aerosol Sources and Processes, *J. Geophys. Res. - Atmospheres* 110:D07S09.

Zhang, Q., Jimenez, J., Canagaratna, M., Allan, J. D., Coe, H., Ulbrich, I., Alfarra, M. R., Takami, A., Middlebrook, A. M., Sun, Y. L., Dzepina, K., Dunlea, E., Docherty, K., DeCarlo, P., Salcedo, D., Onasch, T. B., Jayne, J., Miyoshi, T., Shimono, A., Hatakeyama, S., Takegawa, N., Kondo, Y., Schneider, J., Drewnick, F., Weimer, S., Demerjian, K. L., Williams, P., Bower, K. N., Bahreini, R., Cottrell, L., Griffin, R. J., Rautiainen, J., and Worsnop, D. (2007). Ubiquity and Dominance of Oxygenated Species in Organic Aerosols in Anthropogenically-Influenced Northern Hemisphere Mid-Latitudes, *Geophys. Res. Lett.* 34:L13801.

Zhang, Q., Worsnop, D. R., Canagaratna, M. R., and Jimenez, J. L. (2005). Hydrocarbonlike and Oxygenated Organic Aerosols in Pittsburgh: Insights into Sources and Processes of Organic Aerosols, *Atmos. Chem. Phys.* 5:3289–3311.